A simple parameterization of turbulent tidal mixing near supercritical topography

JODY M. KLYMAK[1], SONYA LEGG[2], AND ROBERT PINKEL[3]
[1]*School of Earth and Ocean Sciences and Department of Physics, University of Victoria, Victoria, Canada*
[2]*Program in Atmosphere and Ocean Sciences, Princeton University, Princeton, NJ, 08544, USA*
[3]*Scripps Institution of Oceanography, University of California, San Diego, La Jolla CA, 98105, USA*

(Manuscript received , in final form)

ABSTRACT

A simple parameterization for tidal dissipation near supercritical topography, designed to be applied at deep mid-ocean ridges, is presented. In this parameterization, radiation of internal tides is quantified using a linear knife-edge model. Vertical internal wave modes that have non-rotating phase speeds slower than the tidal advection speed are assumed to dissipate locally, primarily due to hydraulic effects near the ridge crest. Evidence for high modes being dissipated is given in idealized numerical models of tidal flow over a Gaussian ridge. These idealized models also give guidance for where in the water column the predicted dissipation should be placed. The dissipation recipe holds if the Coriolis frequency f is varied so long as $hN/W \gg f$, where N is the stratification, h the topographic height, and W a width scale. This parameterization is not applicable to shallower topography, which has significantly more dissipation as near-critical process dominate the observed turbulence. The parameterization compares well against simulations of tidal dissipation at the Kauai ridge, but predicts less dissipation than estimated from observations of the full Hawaiian ridge, perhaps due to unparameterized wave-wave interactions.

1. Introduction

Mixing in the ocean provides the potential energy that drives overturning circulations. This mixing tends to be modest in the open ocean, but enhanced near topography. The enhancement can be due to mean-flow interactions with rough topography (as hypothesized by Naveira Garabato et al. 2004), or by internal wave activity generated by tidal forcing (Polzin et al. 1997; Nash et al. 2004; Klymak et al. 2006; Nash et al. 2007), or winds (D'Asaro 1995; Alford 2003).

Parameterizing the mixing due to tidal dissipation is challenging. St. Laurent and Garrett (2002) propose a parameterization which determines the energy transfer to the internal tide by linearizing the forcing following the model of (Bell 1975), an approximation suitable for topographic slopes shallower than the internal tide rays (subcritical topography). St. Laurent et al. (2002) specified a fixed fraction of the baroclinic energy (taken to be 30%) which is dissipated locally around the topography over a fixed vertical scale, taken to be 300m to fit data from several deep ocean sites (St. Laurent and Nash 2004).

While this parameterization is now implemented in several ocean general circulation models (Jayne 2009) several aspects invite improvement: incorporation of new understanding of the transfer of energy to the baroclinic tide at steep, supercritical topography; a physical prediction for the fraction of energy dissipated locally, and a physical prediction for the depth profile of the dissipation. The latter has been tackled for rough topography by Polzin (2004, 2009), using theory for the weakly nonlinear interactions between generated waves and the ambient wavefield.

Here we suggest a parameterization scheme for the tidal mixing near isolated supercritical topography, in which the fraction of energy dissipated locally and depth scale of the dissipation are functions of the topography and flow, rather than arbitrary dimensional constants as in St. Laurent et al. (2002). Simple expressions for internal tidal wave generation over supercritical topography are available by assuming that the topography is an idealized knife edge, or top-hat (St. Laurent et al. 2003; Llewellyn Smith and Young 2003), though more complicated forms allow non-idealized topography (i.e. Balmforth and Peacock 2009). Numerical models and laboratory experiments indicate that these analytical models yield good estimates of tidal generation (Di Lorenzo et al. 2006, and see below).

Previous efforts to estimate the fraction of the energy which dissipates locally include Klymak et al. (2006) which assumed, somewhat arbitrarily, that all the energy

Corresponding author address: J. Klymak, jklymak@uvic.ca

predicted to go into modes 10 and higher was dissipated locally. For varying height ridges, this gave a power law between the dissipation D and the tidal flux F_{M_2} or the tidal energy density E_{M_2}. Observations from a number of locations along the Hawaiian Ridge (Lee et al. 2006) indicated a power law of $D \sim E_{M_2}^{1.3}$. Sampling errors and spring-neap inequalities make this power law very poorly constrained, but it does indicate that the dissipation is not quadratic with tidal energy, which would be the power law predicted by broadband wave-wave interactions (i.e. Gregg 1989).

Here we present a physical argument for determining the fraction of energy dissipated locally: we assume vertical modes with non-rotating phase speeds c_n slower than the peak ridge-top tidal speed, U_m, are assumed to break down into local turbulence (i.e. if $c_n < U_m$). This parameterization is motivated by the observation made in Legg and Klymak (2008) and Klymak et al. (2010) that the mode with $c_n \approx U_m$ is arrested over the topography, becoming turbulent with a hydraulic jump on its lee face. Understanding the vertical length scale of these jumps provides a basis for predicting the vertical decay scale of the local dissipation.

We describe the phenomenology of tidal generation and non-linear breaking waves observed in our numerical simulations (section 3). Then the proposed parameterization scheme is outlined and estimates of local dissipation predicted by this scheme are compared against dissipation simulated in the numerical model (section 4), where the agreement is found to be quite good. Finally, the parameterization is used to estimate dissipation for the Hawaiian Ridge (section 5) and the results discussed (section 6).

2. The numerical model

The proposed dissipation recipe will be calibrated and tested by comparison with simulations using the MITgcm (Marshall et al. 1997). This model has been used for other two-dimensional wave-breaking problems (Legg and Adcroft 2003; Legg and Huijts 2006; Legg and Klymak 2008; Klymak et al. 2010). The model was run in two-dimensions with topography as described below. Forcing was tidal and applied via velocity and density nudging at the boundaries 565 km from the ridge. The model was run using the hydrostatic approximation for numerical efficiency; tests with the non-hydrostatic terms did not reveal substantively different responses for this particular scenario (Klymak and Legg 2010).

The dissipation scheme employed in this model is described in Klymak and Legg (2010), and consists of applying a high vertical viscosity and diffusivity whenever there are density overturns due to breaking waves. The diffusivity is scaled by the size of the density overturns so that the energy loss ε is consistent with the Ozmidov scale L_o

$$\varepsilon = L_O^2 N^3, \tag{1}$$

where N is the stratification after overturns have been removed by density sorting. From this we obtain a turbulent viscosity and diffusivity of $K_v = 0.2\varepsilon/N^2$ or $K_v = 10^{-5}$ m^{2}s^{-1}, whichever is larger. The limitations of this scheme are that it does not account for shear-driven mixing, and it does not work well if the breaking internal waves are small compared to the vertical grid size. However comparisons with more standard dissipation schemes – a local Mellor-Yamada 2.0 scheme (Mellor and Yamada 1982), and constant viscosities (Legg and Klymak 2008) – indicate that this dissipation scheme yields energetically consistent results for the parameter regimes explored here.

The model was usually run with barotropic forcing for 5 tidal cycles. Dissipation and energetics usually settled into steady state in two tidal cycles, though slower waves take longer to propagate through any given control section than the fastest waves. Different ridge cross-sections and barotropic forcings were used, as described in table 1.

3. Phenomenology

Before presenting the parameterization, we briefly review the structure and turbulence of the lee waves observed at supercritical topography. Observations at Hawaii indicate strong bore-like structures propagating near the sea-floor (Levine and Boyd 2006; Aucan et al. 2006; Klymak et al. 2008). These bores are phase locked to the tide, vary strongly with the spring-neap cycle of the semi-diurnal forcing, and contain large turbulent convective overturns. Numerical simulations suggest that the source of the bores at the top of the ridge is from sharp hydraulic jump-like features formed on the downstream side of the ridge crest every tidal cycle. These are swept onridge as the tide relaxes (Klymak et al. 2008; Legg and Klymak 2008).

A numerical example of this flow regime for a Gaussian ridge demonstrates the phenomenon (FIG. 1). The bore from the previous tide can be seen propagating leftwards centered at about 800 m (a) as the tide reverses. As the leftward tide strengthens (b) a lee wave starts to form on the left side of the ridge, and is fully formed and turbulent by (c), after which it propagates to the right with the relaxing tide (d). There are other turbulent patches in the flow, but this lee wave and its subsequent bore provides the bulk of the dissipation.

The character of this instability depends on the overall flow parameters. For oscillatory flow over topography, the important parameters are the stratification, $N(z)$, the frequency ω_o and strength U_o of the barotropic forcing, the water depth, H, and the geometry of the topography (Baines 1995; Garrett and Kunze 2007). For the tides, rotation (Coriolis frequency f) is also important at most latitudes. Here we are interested in topography that represents a steep ridge. We model our topography as an isolated two-dimensional obstacle in a flat-bottom ocean with depth H. The character of the response will depend on the height of this topography h and its aspect ratio $\alpha = h/W$. The aspect ratio is not constant for any natural

Sec.	H[m]	Shape	W [km]	h [m]	$N[10^{-3}\mathrm{s}^{-1}]$	$U_o[\mathrm{ms}^{-1}]$	$\delta z[m]$	δx_{min}[m]	$f[\times 10^{-4}\ \mathrm{s}^{-1}]$
4a	2000	Gaussian	10	500,1000, 1500	5.2	0.04,0.08,...0.24	10	200	1
4b	2000	Gaussian	10	1000	5.2	0.12	10	200	0,1,1.3,1.38,1.4
4c	2000	Gaussian	15,35,55, 75,95,135	1000	5.2	0.12	10	200	1
4e	4320	Gaussian	15	1000	Hawaii	0.55	17-100	273	1
	4320	Kauai Chan.	∼15	1000	Hawaii	0.02,0.035,0.05, 0.055,0.08,0.10, 0.15,0.20,0.30	17-100	273	1,0.5

Table 1: Summary of parameters for model runs in the paper by section. The Hawaiian vertical grid had expanding δz for $z > 2000$m.

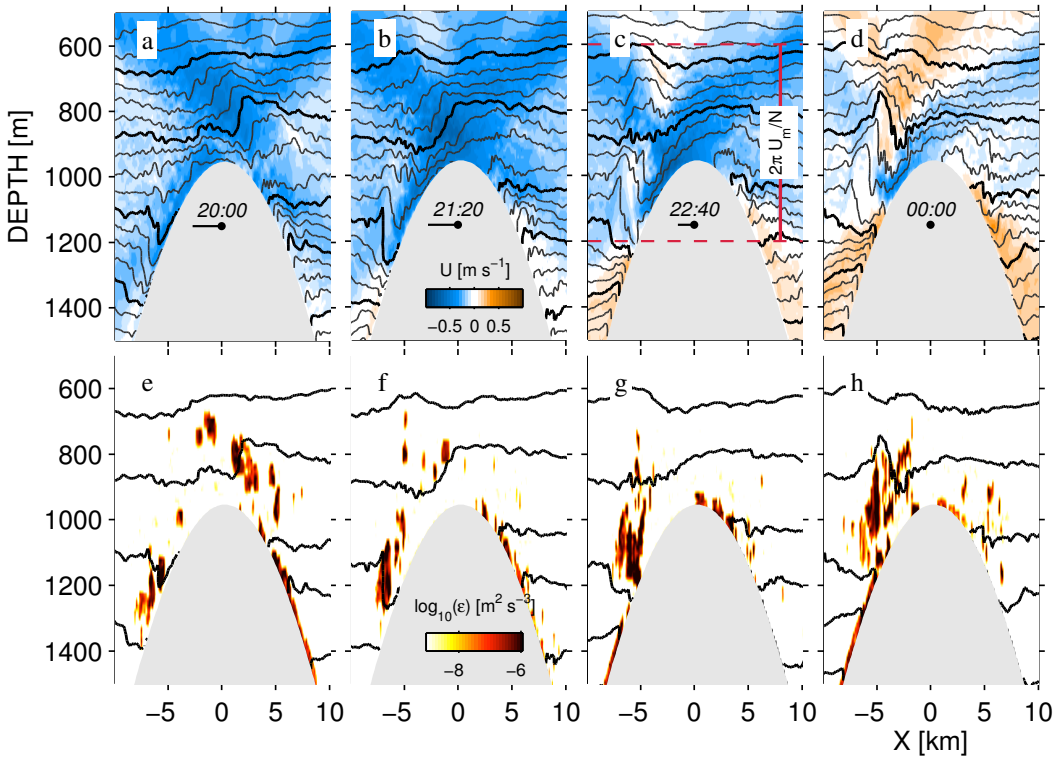

FIG. 1: Simulations of flow over a Gaussian obstacle using a realistic oceanic stratification ($N(z)$ from near Hawaii) and a deep-water ($H = 4300$ m) barotropic velocity amplitude of $U_o = 0.055\mathrm{m\,s}^{-1}$, indicated by the line in each panel. a–d Velocity and isopycnals and e–h turbulence dissipation rate, every 80 minutes as a lee-wave forms on the down-current side of the obstacle crest.

topography; a characteristic aspect ratio can usually be defined, though one needs to be careful what part of the response one is considering when making this definition. For instance, the large-scale response will be determined by the overall shape of the topography, but the turbulent response near the top of the topography will depend on the local topographic slope. An important derived parameter is the slope that a monochromatic internal wave travels relative to the horizontal, given by

$$s = \left(\frac{\omega^2 - f^2}{N^2 - \omega^2}\right)^{1/2}. \qquad (2)$$

If $s > \alpha$ a downward incoming internal wave will reflect in the forward direction off the topography and the topography is called "subcritical". It will reflect if $s < \alpha$ and the topography is termed "supercritical". More importantly

for our problem, internal tides generated at supercritical topography take the form of both upward and downward traveling beams radiating away from the topographic feature, whereas for subcritical topography, waves can only radiate upwards.

There are many places where internal tides (i.e. ω_o is at tidal frequencies) are supercritical to the topography, and that is the focus here. We also are interested in flows where $Nh/U_o \sim O(10-1000)$, so that the characteristic Froude number of the lowest modes is small. As mentioned above, and we will show below, such flows have proven amenable to linear theory for predicting the bulk of the response. However, here we are interested in the local turbulence dissipation, where the linear response breaks down.

The character of the lee wave that forms over supercritical topography can be predicted from a simple steady-state scaling (Klymak et al. 2010) that demonstrates that the lee wave is arrested by the oncoming barotropic flow at the top of the ridge such that $c_x = U_m = U_o H/(H-h)$. In the non-rotating limit, the arrested wave has a vertical wavelength

$$\lambda_z \approx 2\pi U_m/N = 2\pi \frac{U_0 H}{dN} \tag{3}$$

(where $d = H-h$) (FIG. 1c). Waves with this vertical wavelength are the smallest that can escape from the sill, and waves with smaller vertical wave-lengths are trapped and dissipate locally. As the steady-state forcing is increased, the lee-waves get larger, and a greater range of wavelengths are arrested.

The horizontal wavelength of the turbulent lee wave is set by the aspect ratio of the topography $\alpha = h/W$, where W is a width scale (Klymak et al. 2010). This means that for a constant-stratification non-rotating ocean the lee wave has a frequency given by the hydrostatic dispersion relation $\omega_{lee} = Nk_x/k_z \approx N\alpha$ (Klymak et al. 2010). For an oscillatory flow such as that driven by a barotropic tide, a vigorous lee wave only forms if there is enough time for the vertical signal to propagate in the vertical before the tide shifts, so $\omega_{lee} > 2\omega_o$ (Klymak et al. 2010), which means that the ridge must be super-critical enough so that $N\alpha > 2\omega_o$. For near-critical ($N\alpha < 2\omega_o$) ridges, turbulent lee waves are not expected to form and other physics takes over (Legg and Klymak 2008, as demonstrated below, section 4c). Steep topography, so that $\omega_{lee} > 2\omega_o$, also means that for most latitudes $\omega_{lee} \gg f$, and the turbulent lee waves are not strongly affected by rotation; the non-rotating dispersion relation still applies.

We can test numerically our prediction that wavelengths smaller than $\lambda_c = 2\pi\frac{U_0 H}{dN}$ are dissipated locally. First we compare two representative runs in a constant stratification ocean ($N = 5.2\times10^{-3}$ s^{-1}), $h/H = 0.5$, and $\alpha = 0.1$ (FIG. 2). When the tidal forcing is doubled from $U_o = 0.08$ to $U_o = 0.16$ m s^{-1}, λ_c is doubled. A larger lee wave is evident on the right side of the sill in the more strongly-forced run. The main tidal beams radiating from the ridge crest are thicker and less focused in the more strongly forced run, indicating a dominance of larger vertical wavelengths. This can be demonstrated more quantitatively by comparing the energy flux as a function of vertical mode number in several different simulations.

Simulation parameters are given in table 1. To examine the distribution of energy in different vertical modes as a function of forcing velocity, the modal content of the energy flux is evaluated from the model results. Baroclinic velocity u' and pressure p' fluctuations are decomposed into vertical modes, integrating their product and averaging over a tidal period:

$$F_n = \int_{-H}^{0} < u'_n p'_n >_{tide} \, \mathrm{d}z. \tag{4}$$

Six model runs for three of the ridge heights are presented where the only variable is the tidal forcing U_o (FIG. 3). We also compare the simulated energy flux 15 km from the obstacle crest with the theoretical prediction for a knife-edge topography (St. Laurent et al. 2003; Llewellyn Smith and Young 2003) in which the energy flux depends quadratically on the tidal forcing:

$$F_n = U_o^2 \, \mathcal{F}\,(n, N(z), h, H) \tag{5}$$

(see the following section for more detail). In this theoretical prediction, the distribution of the flux among modes only depends on the geometry and stratification, not the strength of the forcing.

For low modes, the knife-edge model predicts the energy content quite well. However, as the modenumber increases, the linear model overestimates the energy flux. Some of this overestimation is because the higher modes, even if they escape the ridge, or are produced mid-water column by other interactions, do not have time to reach the edge of our domain. However, time dependence of this roll off should be the same for all the model runs, regardless of U_o, whereas the results demonstrate that stronger flows roll off at lower wavenumbers than weaker flows. For instance, for $h = 1500m$, the 0.04 m s^{-1} flux rolls off at mode 11, whereas the strongly-forced 0.24 m s^{-1} rolls off almost at mode 2. The differences are more subtle for the smaller ridges, but the same pattern is evident.

To summarize, for a given stratification and flow geometry, larger forcing implies:

- Larger breaking lee waves, leading to more turbulence
- A smaller fraction of high-mode content radiating away from the ridge.

We use these theoretical arguments and model results to make a simple parameterization for the dissipation near the ridge, and then attempt to verify it by comparison with our numerical simulations and the observations at Hawaii.

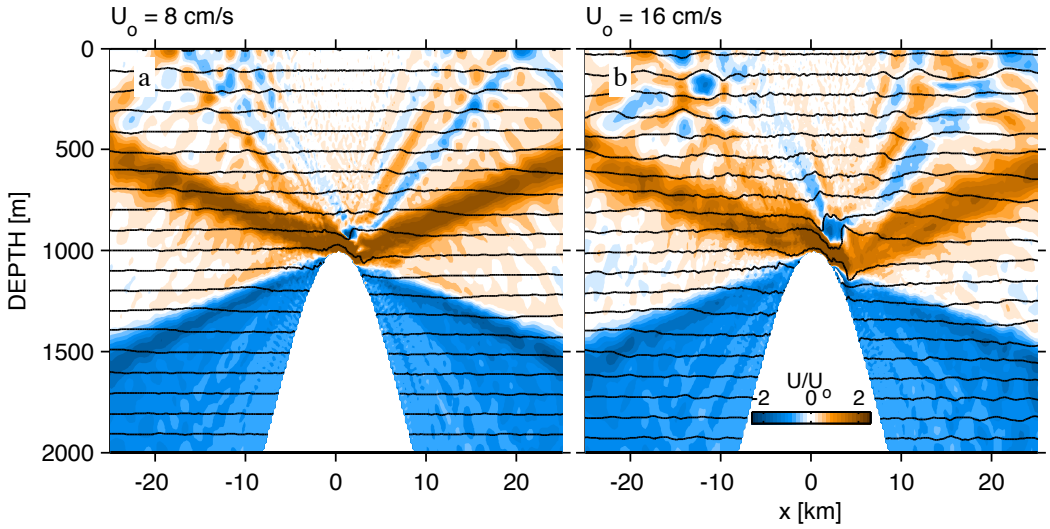

FIG. 2: Baroclinic velocity at hour 57 in runs with $U_o =$ a) 0.08 $\mathrm{m\,s^{-1}}$ and b) 0.16 $\mathrm{m\,s^{-1}}$. Both velocities have been scaled by the forcing velocity and have the instantaneous deep-water barotropic velocity removed. Note the larger lee wave in the faster simulation. Also note that beams radiating from the ridge crest in the faster simulation are less well-defined compared to the slower simulation.

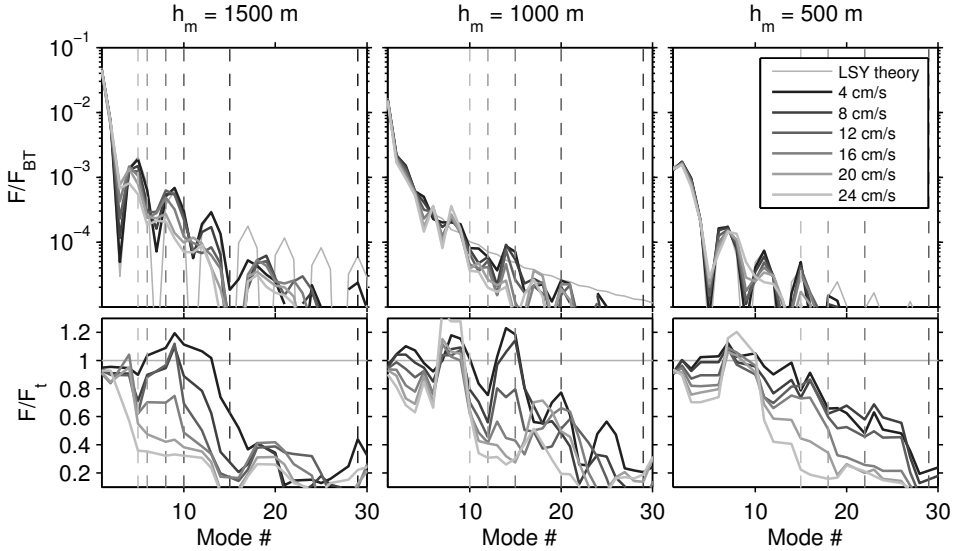

FIG. 3: Energy flux for three different ridge geometries and six different barotropic tidal forcings time-averaged over tidal periods 4 and 5. The flux is sum of energy out of a region bounded laterally by $x = \pm 15$ km. The upper row shows the observed flux (shaded lines) and the theoretical flux (thin gray lines) normalized by the flux in the barotropic tidal wave while the lower row shows the observed response divided by the theoretical response. This ratio is only computed for the peak modes in the theoretical response, not the nulls, and has been smoothed by three adjacent modes to make the response trend a little clearer.

4. The parameterization and numerical tests

Our new parameterization for the turbulence dissipation at isolated steep topography is based on the premise

that the mode number corresponding to the vertical wavelength of the arrested horizontally propagating mode is the largest that can escape from the sill. Any higher vertical modes are trapped and dissipate locally. For a constant-stratification ocean, the deep-water vertical mode corresponding to the lee-wave vertical wavenumber is approximated by

$$n_c \approx \frac{NH}{\pi U_m} = \frac{Nd}{\pi U_o}. \tag{6}$$

As the tidal forcing is increased, the lee waves get larger, more modes are arrested and we expect more local dissipation.

We now formulate this premise into a simple recipe for the turbulence dissipation. Given a water depth H, a maximum obstacle height h, a stratification $N(z)$, and a cross-topography tidal forcing U_o, we derive a volume-integrated dissipation D. First we note that the internal wave response can be described by the deep-water vertical modes that are specified uniquely in terms of H and $N(z)$. Each mode, indexed by n, has a distinctive vertical shape and eigenspeed, c_n, attainable numerically (Gill 1982), with $c_1 > c_2 > c_3 > ....$ If N is a constant, then

$$c_n = \frac{NH}{n\pi}. \tag{7}$$

The eigenspeed, c_n, is also the phase and group speed of the lee waves in the hydrostatic non-rotating limit because $\omega_{lee} \gg f$ (we test that this is an appropriate limit below, section 4b).

To estimate the energy flux generated in each mode, F_n, we use a simple knife-edge model (Llewellyn Smith and Young 2003, hereafter LY03)[1]. Working in a WKB-stretched co-ordinate system:

$$Z = \frac{\pi}{H}\int_0^z N(z')/\langle N(z)\rangle \, \mathrm{d}z'. \tag{8}$$

If the height of the ridge from the seafloor is h in real co-ordinates and B in stretched co-ordinates, then the production of internal wave energy is (LY03 eq 5.12)

$$F = \frac{\pi}{4}\rho_0 U^2 \sqrt{1-\frac{f^2}{\omega^2}} N(h)\, h^2\, \mathcal{M}, \tag{9}$$

where $\mathcal{M}(B/\pi)$ is given by:

$$\mathcal{M}(B/\pi) = \frac{4}{\pi B^2}\int_0^B Z\sqrt{\frac{1-\cos Z}{\cos Z - \cos B}}\mathrm{d}Z. \tag{10}$$

As pointed out by LY03, this is best evaluated numerically with the substitution $t = \tan(Z/2)$, which makes the integral:

$$\mathcal{M}(B/\pi) = \frac{16\sqrt{1+\tau^2}}{\pi B^2}\int_0^\tau \frac{t\tan^{-1}t}{\sqrt{\tau^2-t^2}}\frac{\mathrm{d}t}{1+t^2}. \tag{11}$$

[1]This model gives identical results to the geometric model given by St. Laurent et al. (2003) but is computationally faster, and of similar complexity to set up numerically

The projection of F onto vertical modes is derived as:

$$F_n = F\, n^{-1}\mathcal{P}_n^2 / \sum_{k=1}^{\infty} k^{-1}\mathcal{P}_k^2 \tag{12}$$

where $\mathcal{P}_k = P_{k-1}(\cos B) - P_k(\cos B)$, and P_k is the kth Legendre polynomial.

The local dissipation is calculated assuming that the modes that have c_n slower than U_m do not escape the ridge and instead dissipate locally so that

$$D = \sum_{n_c}^{\infty} F_n \tag{13}$$

where n_c is chosen so that $c_{n_c} < U_m$. This corresponds to the speed of the breaking lee wave seen in the simulations above and indicated by the observations at Hawaii (Klymak et al. 2008).

a. Tests with constant stratification and Gaussian topography

We now have a prediction for D, the total local dissipation: for implementation in a coarse resolution numerical model we will need to prescribe a vertical and horizontal distribution of this dissipation. First however, we will verify that this prediction for the total dissipation agrees with results from high-resolution numerical simulations of tidal flow over a Gaussian topography (table 1).

The turbulence dissipation, ε, was integrated over a 30-km wide region centered on the Gaussian ridges. This simulated estimate, D_{Model}, was compared with the dissipation predicted from the parameterization recipe (D_{Param}, FIG. 4). We cover three orders of magnitude of baroclinic generation with these simulations, and almost four orders of magnitude in the predicted dissipation rate. The dissipation rate observed in the numerical model scales quite well with that predicted by the recipe, with the parameterization slightly over-predicting for most runs, with a mean over-prediction of 1.1.

It is useful to note that the dissipation in both the parameterization and the numerical model scales with U_o^3 (FIG. 5). We can show this by noting that

$$F_n \sim \frac{U_o^2}{n^2} \tag{14}$$

If we allow n to be continuous then

$$D \sim \int_{n_c}^{\infty} F(m)\,\mathrm{d}m \tag{15}$$

$$\sim \frac{U_o^2}{n_c} \tag{16}$$

and we note that according to the parameterization $n_c = \frac{(H-h)N}{U_o\pi}$, so

$$D \sim U_o^3 \tag{17}$$

$$\sim U_o \nabla F, \tag{18}$$

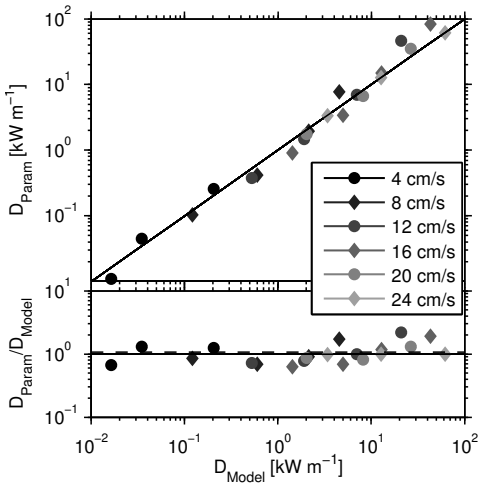

FIG. 4: Test of parameterized dissipation D_{Param} compared to the dissipation in the numerical model D_{Model}. The same deep-water barotropic forcing was run over Gaussian ridges with 4 different heights. The mean ratio of the parameterization and the numerical model dissipations is 1.1, and indicated with a dashed line.

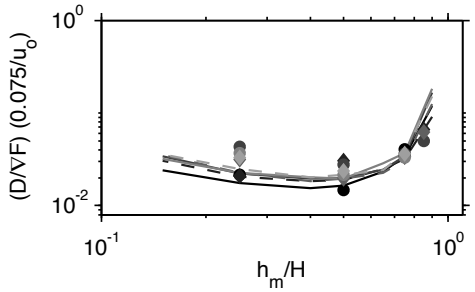

FIG. 5: Comparison of the dissipation parameterization (lines) and the dissipation in the numerical model (symbols) as a function of ridge height, almost collapsed onto a single curve by noting that the dissipation scales with U_o^3.

where ∇F is the horizontal divergence of the depth-integrated energy flux. This allows us to remove the spread between differently forced models to compare all the runs on an almost-collapsed curve (FIG. 5).

b. Dependence on rotation

The simulations above were run with $f = 10^{-4}$ s^{-1}. We chose our critical mode based on the hydrostatic non-rotating phase speed c_n rather than its hydrostatic tidal-frequency counterpart $c_p = c_n\omega/(\omega^2 - f^2)^{1/2}$. We justified this on the basis that the non-linear lee waves in steady state are observed to have intrinsic frequencies $\omega_{lee} = \alpha N$ (Klymak et al. 2010). For the topography above $\omega_{lee} \approx 5.2\times10^{-4}$ s^{-1}, so the rotating $c_{lee} = 1.02c_n$ for $f = 10^{-4}$ s^{-1}, and the hydrostatic non-rotating eigenspeed, c_n, can be used without changing the results. Conversely, the tidal phase speed would be $1.42c_n$, and dissipation would be greatly reduced as more modes would be free to propagate from the ridge.

This is verified by changing f and comparing the theory with the simulations (FIG. 6). The energy flux put into the tides varies with the group speed, $c_g = c_n(\omega^2 - f^2)^{1/2}/\omega$ (equation (9)), so higher-f simulations have less energy flux (FIG. 6a, upper curve). They correspondingly have less dissipation, both as observed in the model and with the theory of $c_{n_c} \approx U_m$ (FIG. 6a, lower lines and symbols). If we instead had said that modes dissipated are governed by the tidal phase speed, $c_{p_c} \approx U_m$, then much less dissipation would be predicted at high latitudes (FIG. 6a, thin dashed line) as more modes would be fast enough to escape.

The justification for the scaling is borne out by considering snapshots of the response as f is increased (FIG. 7). For all these runs $2\pi N/U_m = 290$m. When normalized by the total expected dissipation, the structure of ε is approximately the same for these runs, with a halo approximately 150 m above and below the obstacle crest, and a trapped response of approximately this vertical wavenumber is evident in all four examples. The non-linearity of the response is less as f is increased (i.e. FIG. 7d versus a) because less energy is put into the wavefield.

Topography with a gentler aspect ratio may have lee waves more affected by rotation as ω_{lee} drops closer to f, and we might expect to see turbulence drop. That is not the case, however, as topographies shallow enough to have this effect start to develop turbulence due to near-critical processes, as discussed next.

c. Width dependence

Our parameterization is intended only for supercritical topography, $\omega_{lee} > 2\alpha N \gg f$, when the lee-wave breaking is the dominant dissipation process. If the slope approaches critical steepness, for example by increasing the width while keeping the height constant, dissipation increases (FIG. 8). There is another process at work here that the supercritical generation/dissipation model is not intended to parameterize. On the "near-critical" part of the obstacle slope, where $dh/dx \approx \omega/N$, the wave characteristic lies along the slope, and upslope bores form. This process has been studied in the laboratory (McPhee and Kunze 2002) and there is evidence for it in nature (Gemmrich and van Haren 2001; Aucan and Merrifield 2008). The more of the slope that is "near-critical", the more important to the local dissipation these upslope bores become (FIG. 8a–d). For subcritical flow (FIG. 8f), the dissipation from the topography is negligible. Our parameterization is not intended to apply in either of the

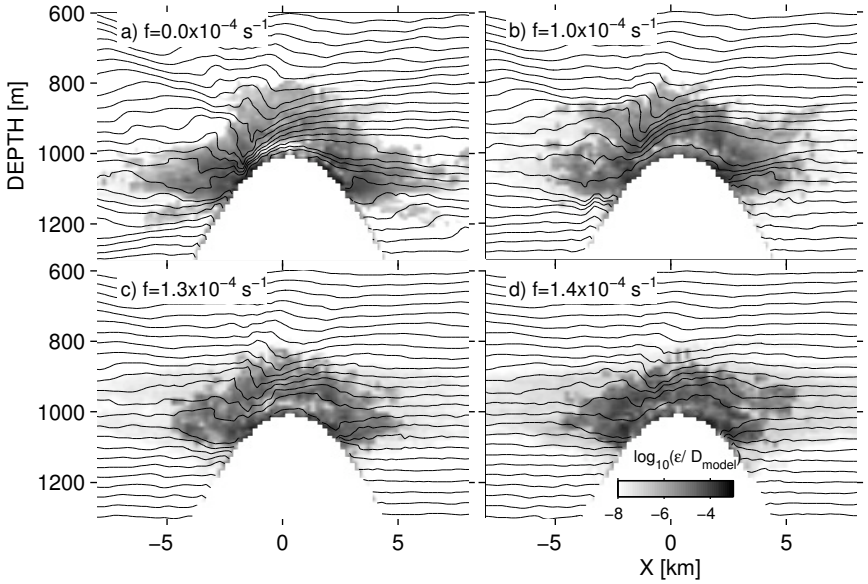

FIG. 7: Character of the response as rotation is increased. Density is contoured; Shading is the logarithm of the dissipation, scaled by the total dissipation.

near-critical or subcritical regimes, and any implementation should be conditional on supercritical topography.

d. Vertical decay scale of dissipation

The region with the most significant dissipation is confined near the crest of the topography, within half a wavelength below and above the ridge crest (FIG. 9), where the wavelengths scale as $\lambda_o = 2\pi U_m/N$ (Klymak et al. 2010). If we define

$$e(z) = \frac{\lambda_o}{D}\int \varepsilon(x,z)\,\mathrm{d}x, \tag{19}$$

we find that the horizontal integral from $x = -15$ km to 15 km of the dissipation collapses significantly when plotted versus z/λ_o. This scale is rough, but probably adequate for using this parameterization of the dissipation in coarser resolution models. Horizontally, the turbulence is confined to the top of the slope, presumably within a horizontal grid cell if these effects are being parameterized in a larger scale model.

We fit a very simple model to this depth dependence: We set the dissipation to peak at $-0.15\lambda_0$ below the obstacle crest, and to decay exponentially above and below such that it reaches 0.001 of its max $0.65\lambda_0$ below the crest and 0.01 of its max $0.65\lambda_o$ above (FIG. 9). This fit is not exact, but distributes the dissipation fairly well, and is adequate for a simple model like this. Importantly, it does not introduce any new dimensional parameters, with the dissipation decay scale being dependent on the known parameters of the flow.

e. Numeric tests with realistic stratification and Hawaiian topography

Having shown that the parameterization of dissipation compares well with simulated dissipation for idealized Gaussian topographies, we now compare with simulations using more realistic topography and stratification, although we retain the two-dimensional assumption. We use the same cross-section and stratification as Legg and Klymak (2008) from the Kauai channel between Oahu and Kauai in the Hawaiian islands.

We first note that the idealization to Gaussian topography yields quite accurate results (FIG. 10). The total energy lost from the barotropic tide is almost identical for the two shapes. The response near the ridge is more complicated in the realistic case, and there is more dissipation, but the increase is only 25%, which, given the crudeness of our scheme, is likely an acceptable error.

We apply the same recipe as above with a WKB-stretched version of the knife-edge generation model and compare to the output from different forcing over the realistic ridge (FIG. 11). Again the recipe does a good job of predicting the dissipation, with a small over prediction. The same U_o^3 power law is obtained as for the Gaussian cases discussed above.

Finally, these "Hawaiian" runs were made with $f = 10^{-4}$ s^{-1}, appropriate for mid latitudes. Equatorward of 28.8°, where $f < \omega_o/2$, internal waves are susceptible to a class of wave-wave interactions termed parametric subharmonic instabilities (PSI) that tend to be faster than other wave-wave interactions poleward (McComas and Müller 1981; MacKinnon and Winters 2005; Carter

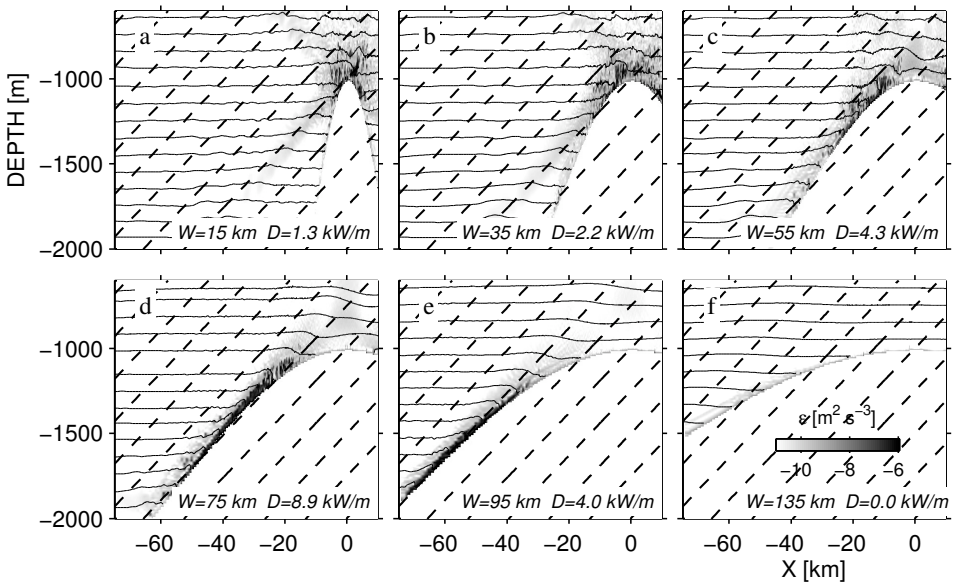

FIG. 8: Change of dissipation as topography becomes wider. Tidal flows over Gaussian topographies, $U_o = 0.12$ m s^{-1}, with widths given in table 1. Dashed lines are characteristic slopes for the tide (equation (2)). As topography approaches critical, upslope bores dominate the signal, rather than the lee-waves parameterized here.

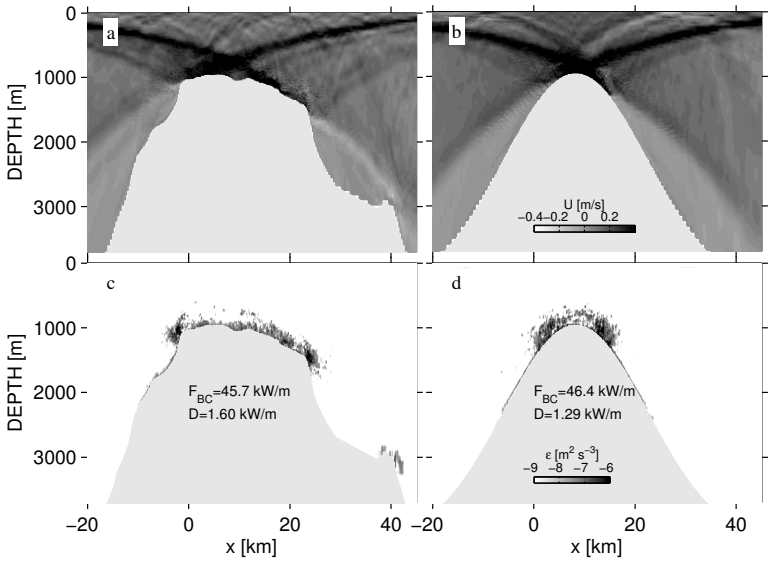

FIG. 10: Comparison of Kauai Channel bathymetry to an idealized Gaussian for $U_o = 0.055$ m s^{-1}, $f = 10^{-4}$ s^{-1}, and realistic Hawaiian stratification $N(z)$. a) and b), velocity snapshots, and c) and d) tidally averaged dissipation. Note the realistic topography dissipates 25% more energy than the Gaussian.

and Gregg 2006). The Hawaiian Ridge is south of this latitude, so we check the response with $f = 10^{-5}$ s^{-1} (FIG. 12). After allowing the model to spinup for 8 tidal cycles, there is more shear, particularly in the tidal beams, which appear particularly susceptible to PSI. At this stage of the model, this shear is not sufficient to drive overturns that are resolved as large turbulent events, and, in fact, the dissipation is slightly less than for the northern sim-

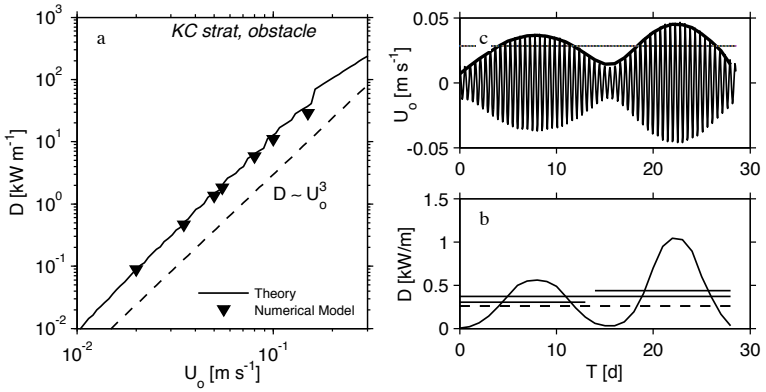

FIG. 11: a) Dissipation (D) in simulations of flow over the Kauai Channel topography and stratification, for seven different barotropic forcings (triangles). The result of the recipe is shown as a solid line, and a cubic power law is shown for comparison. b) and c) compare what would happen in a typical spring neap cycle to aliased averages.

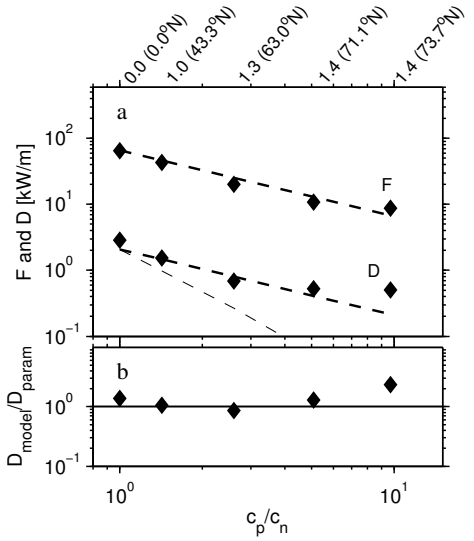

FIG. 6: Idealized model runs varying f. a) Energy fluxes away from the topography compared with the knife-edge theory (upper lines and dots) and dissipation compared with the theory present ed here (lower lines and dots). The thinner dashed curve indicates what the dissipation would be if the arrested wave had a phase speed set by ω_{M_2} rather than ω_{lee}. b) ratio of the modeled dissipations and the theory.

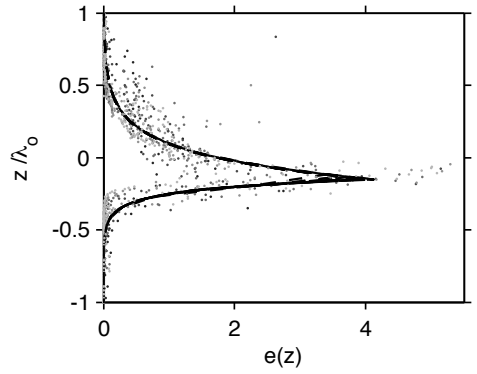

FIG. 9: Depth dependence of the dissipation; a simple exponentially decaying model is shown with dashed lines. Points show horizontally integrated dissipation from all simulations, scaled by D/λ_0, where D is the total dissipation and $\lambda_0 = 2\pi U_m/N$.

ulation. The subgridscale representation of dissipation in the simulations we ran does not have a shear instability component to it, so the only dissipation due to shear mixing is due to the relatively small background viscosity of $K_\nu = 10^{-5}$ m^2 s^{-1}. Including wave-wave interactions is beyond the scope of the present model, but may be important. We anticipate that a full parameterization of mixing processes due to tides will need to include both the lee-wave processes and the wave-wave interactions such as PSI.

5. Example Application to the Hawaiian Ridge

a. Application to a two-dimensional Kauai Channel

The numerical work above encourages us to compare the predictions from our new recipe with observations of dissipation made at the Hawaiian Ridge. Much of the data from the ridge was collected in a two-dimensional slice along Kauai channel. At this location, observations indicate that approximately 40 kW/m of energy radiated

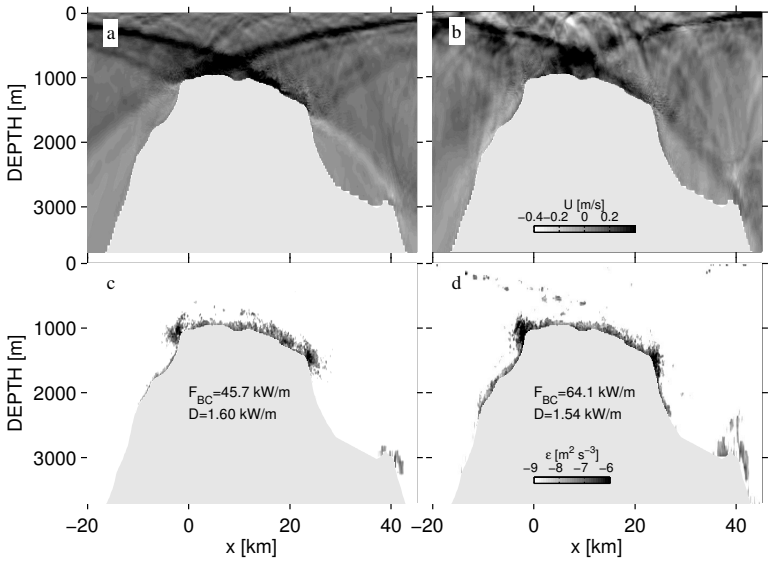

FIG. 12: As for FIG. 10, except b) and d) are for a latitude more suitable for Hawaii, $f(20N) = 5 \times 10^{-5}$ s^{-1}.

away from the ridge as propagating internal waves (Lee et al. 2006). Klymak et al. (2006, K06) used vertical profiler measurements on top of the ridge and at the 3000-m isobath to infer a vertical decay scale of the turbulence that scaled with total water depth. Horizontal towed measurements were used to infer an off-ridge decay scale. They then assumed that the dissipation was separable in the vertical and horizontal and made a synthetic field of total dissipation at the site, which summed to 3.2 kW/m when both sides of the ridge are accounted for.

For the recipe proposed here, the M_2 tide has a barotropic value in the deep water of $U_o \approx 0.045$ m s^{-1}, in $H = 4300$ m of water and a ridge height $h \approx 3000$ m. The recipe agrees with the observations and predicts that 40 kW m^{-1} of energy is lost from the barotropic tide (FIG. 13). All modes higher than 16 are slower than the ridge-top tidal amplitude $U_m = 0.19$ m s^{-1}, and are predicted by the recipe to dissipate, yielding 1.3 kW m of predicted dissipation. This is less than half the 3.2 kW m suggested by K06. We discuss this discrepancy below, but do not immediately discount our parameterization in light of the level of extrapolations made in K06.

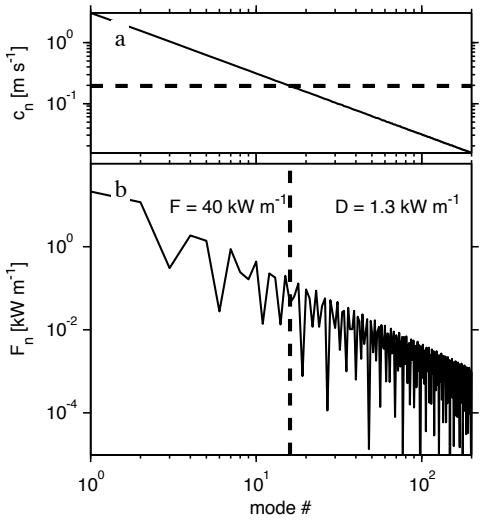

FIG. 13: Recipe applied to Kauai Channel. a) wave speed, with U_m indicated as a dashed line. b) energy flux as a function of mode number, with the fastest "trapped" mode indicated with a dashed line.

b. Application to the whole ridge

The same procedure can be applied to the whole ridge, which has varying ridge heights h and tidal forcing U_o. First, as a groundtruth, we apply the model to varying ridge heights, holding $U_o = 0.04$ m s^{-1} constant. A rough power law between local dissipation and tidal energy density was found at the ridge (Lee et al. 2006) where $D \sim E^{1.3}$. We can compare with the energy density in the recipe ($E_n = F_n/c_n$) and find a similar power law for ridges of varying heights (FIG. 14). We also compare this to the more naive model put forward by K06 that all modes higher than 10 dissipate, regardless of forcing. That simpler model predicts stronger dissipation, and slightly less dependence on the energy density that was observed. Of course the data is necessarily a rough comparison, and derived from localized measurements

taken at the 3000-m isobath, however, it is encouraging that the data and model have similar power laws[2].

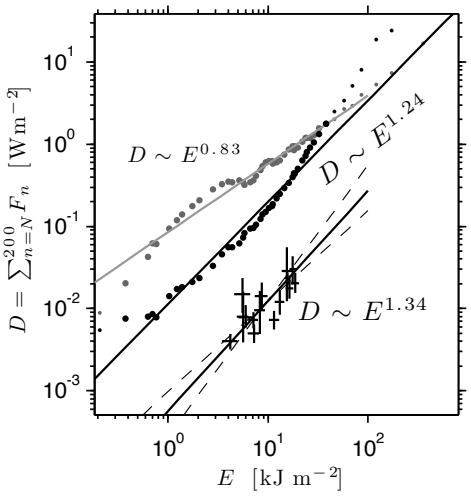

FIG. 14: Power law of dissipation compared to internal wave energy density for, crosses: data collected along the 3000-m isobath (Lee et al. 2006); dark dots: recipe proposed in this paper; light dots: a simpler version of this recipe, where all energy above mode 10 is dissipated.

To extend the recipe to two dimensions we consider the topography at the ridge and the barotropic velocities predicted by the Oregon State Tidal Model (OTIS Egbert and Erofeeva 2002). The bathymetry and velocities are smoothed by 25 km and then the velocity and depth at the shallowest portion of the topography are determined (U_m and h). The barotropic forcing is calculated from the ridge-top velocity $U_o = U_m h/H$, where $H = 4500$ m, the deep water depth away from the sharp topography. This yields a total dissipation from the bathymetry in agreement with the losses suggested by Egbert and Ray (2003) of about 20 GW, similar to estimates made by St. Laurent et al. (2003) and Llewellyn Smith and Young (2003) for knife-edge topographies, though they used one ridge height and velocity to make their estimates. Here the agreement is over the whole ridge using realistic water depths and velocities. Regions of strong forcing stand out, in particular Kauai Channel and French Frigate Shoals, though the values at KC are somewhat less than the ≈ 30 kW/m observed (Lee et al. 2006), though very similar to the ≈ 20 kW/m modeled by (Merrifield and Holloway 2002), indicating that the ≈ 30 kW/m might be slightly exaggerated by spring-neap modulation of the D_2 signal.

[2]Note that the amplitudes are not comparable when comparing the data in FIG. 14 to the observations; the observations are a profile average, whereas the data are a cross-section average. We compare the power laws under the assumption that the scaling is linear in the cross-section dimension.

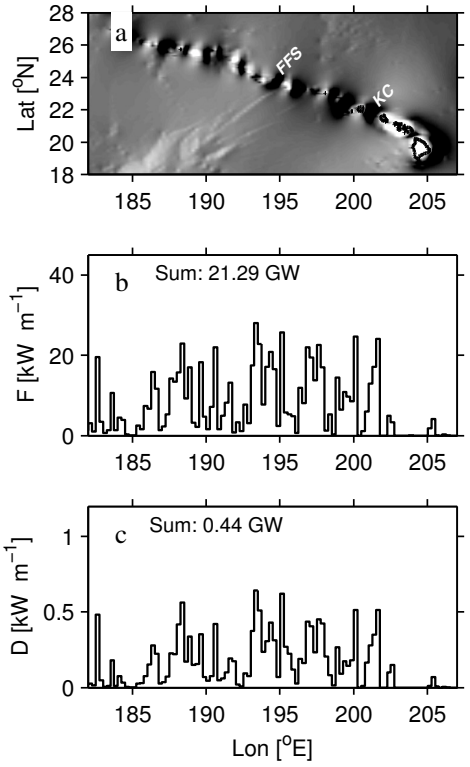

FIG. 15: Application of the knife edge model and dissipation recipe to the whole ridge. a) image of barotropic tidal velocities used for the model. b) baroclinic internal tide flux as a function of along-ridge distance, c) dissipation as a function of along-ridge distance.

The dissipation recipe predicts only 2% of the energy removed from the barotropic tide goes into local turbulence dissipation for the ridge as a whole, emphasizing the efficiency of this type of topography in generating linear internal waves. This low fraction is significantly lower than the 3 GW out of 20 GW estimated by K06, which is about 14%. The difference could be accounted for by

- No wave-wave interactions are present in either the new parameterization recipe or the sub-grid-scale scheme in the numerical model.
- A 2D representation of the breaking waves at the ridge ignores focusing and perhaps underestimates the observed breaking and turbulence.
- The simple extrapolation to poorly-measured parts of the 2-D topography used by K06 exaggerated the importance of flank turbulence. The spring-neap cycle of the forcing also implies a U^3 dependence on the dissipation (FIG. 11b) leading to the possibility of significant sample bias.

- K06 used the power law between D and E, and E from the numerical model by Merrifield and Holloway (2002). It is possible that the along-ridge estimate of E from the numerical model was not an accurate proxy for local dissipation.

6. Discussion

We have presented a simple recipe for parameterizing the dissipation of internal tidal energy generated at steep topography. The recipe uses a linear model appropriate for steep topography to estimate the energy lost from the barotropic tide and the modal content of the internal wave field. Modes that are slower than the local velocity at the top of the topography are then assumed to dissipate, faster modes are allowed to propagate away from the topography. We tested this numerically for both idealized topography and realistic two-dimensional topography and find that the local dissipation is well-predicted from the recipe. Application to the Hawaiian Ridge yielded significantly lower estimates than those published by K06, but it is not clear that the observational estimates are robust enough to fully test the model.

The justification for the scheme comes from Klymak et al. (2010) where it is shown that the lee waves that form each tide have the non-rotating phase speed $c_n \approx U_m$. This scaling has some appeal, even if lee waves are not the only dissipative mechanism, as it means slow waves are dissipated locally, and fast ones escape. Regardless the numerical simulations support the parameterization recipe for this phenomena. However, the recipe would under-predict the dissipation if the tidal-frequency phase-speed were used, a consequence of the trapped waves having a higher intrinsic frequency than the tidal forcing.

The implications of the parameterization scheme are

- total dissipation scales like the cube of the barotropic velocity: $D \sim U_o^3$
- moderate-depth ridges with slow forcing are highly efficient at radiating internal tides, so that the fraction of energy dissipated locally is small.

Since such a low fraction of the energy goes into local dissipation, it may not be worth applying the dissipation portion of this parameterization for many locales. However, there are regions of fast forcing and shallow ridges where the local dissipation may be more substantial, such as the Luzon Strait, connecting the South China Sea to the Pacific. It also means that models that put the localized mixing at a fixed 30% of the local generation (e.g. St. Laurent et al. (2002)) are likely to exaggerate the local topographic mixing.

The question of where the energy propagates to and ultimately dissipates is the next step of this research. Scattering of the internal tide, either at subsea topography (Johnston and Merrifield 2003), or continental slopes (Nash et al. 2004, 2007) is thought to be important. The same simplified geometry and linear theory can be applied to the transmission-reflection problem of a mode-1 wave approaching topographic obstacles, so determining which of the scattered modes is likely to escape the topography seems like a plausible way to proceed.

The numerical model and parameterizations agree quite well with each other, but seem to have less dissipation than observations indicate for the Hawaiian ridge. Part of the shortfall of dissipation may be due to poorly resolved observations, but it is also possibly because the parameterization does not have wave-wave interactions in it. Recently, Polzin (2009) has suggested a vertical balance for the internal wave generation/dissipation problem. For supercritical topography, we conceptualize the waves radiating horizontally from an isolated piece of topography, but it seems plausible that wave-wave interactions could be added to the breaking-wave recipe.

Acknowledgements. We would like to thank Eric Kunze and two anonymous reviewers for helpful comments. This work arose from the NSF-funded Hawaiian Ocean Mixing Experiment, and we thank the scientists involved in that experiment. JK was supported by ONR grants N00014-08-1-0376 and N00014-08-1-0274 and NSERC grant 327920. RP was supported under National Science Foundation grant NSF OCE 98-19529. SL was supported by award NA08OAR4320752 from the National Oceanic and Atmospheric Administration, U.S. Department of Commerce. The statements, findings, conclusions, and recommendations are those of the author(s) and do not necessarily reflect the views of the National Oceanic and Atmospheric Administration, or the U.S. Department of Commerce.

References

Alford, M. H., 2003: Improved glogal maps and 54-year history of wind work on ocean inertial motions. *Geophys. Res. Lett.*, **30**, doi:doi:10.1029/2002GL016614.

Aucan, J., and M. A. Merrifield, 2008: Boundary mixing associated with tidal and near-inertial internal waves. *J. Phys. Oceanogr.*, **38**, 1238–1252.

Aucan, J., M. A. Merrifield, D. S. Luther, and P. Flament, 2006: Tidal mixing events on the deep flanks of Kaena Ridge, Hawaii. *J. Phys. Oceanogr.*, **36**, 1202–1219.

Baines, P. G., 1995: *Topographic Effects in Stratified Flows*. Cambridge Univ. Press, New York.

Balmforth, N. J., and T. Peacock, 2009: Tidal conversion by supercritical topography. *J. Phys. Oceanogr.*, doi:10.1175/2009JPO4057.1.

Bell, T. H., 1975: Topographically generated internal waves in the open ocean. *J. Geophys. Res.*, **80**, 320–327.

Carter, G. S., and M. C. Gregg, 2006: Persistent near-diurnal internal waves observed above a site

of M_2 barotropic-to-baroclinic conversion. *J. Phys. Oceanogr.*, **36**, 1136–1147.

D'Asaro, E. A., 1995: Upper-ocean inertial currents forced by a strong storm. Part II: Modeling. *J. Phys. Oceanogr.*, **25**, 2937–2952.

Di Lorenzo, E., W. R. Young, and S. Llewellyn Smith, 2006: Numerical and analytical estimates of m_2 tidal conversion at steep oceanic ridges. *J. Phys. Oceanogr.*, **36**, 1072–1084.

Egbert, G. D., and S. Y. Erofeeva, 2002: Efficient inverse modeling of bortropic ocean tides. *J. Atmos. Ocean. Tech.*, **19**, 183–204.

Egbert, G. D., and R. D. Ray, 2003: Semi-diurnal and diurnal tidal dissipation from TOPEX/Poseidon altimetry. *Geophys. Res. Lett.*, **30**, 1907, doi:10.1029/2003GL017676.

Garrett, C., and E. Kunze, 2007: Internal tide generation in the deep ocean. *Ann. Rev. Fluid Mech.*, 57–87.

Gemmrich, J. R., and H. van Haren, 2001: Thermal fronts generated by internal waves propagating obliquely along the continental slope. *J. Phys. Oceanogr.*, **31**, 649–655.

Gill, A. E., 1982: *Atmosphere-Ocean Dynamics*. Academic, 662 pp.

Gregg, M. C., 1989: Scaling turbulent dissipation in the thermocline. *J. Geophys. Res.*, **94**, 9686–9698.

Jayne, S. R., 2009: The impact of abyssal mixing parameterizations in an ocean general circulation model. *J. Phys. Oceanogr.*, **39**, 1756–1775.

Johnston, T. S., and M. A. Merrifield, 2003: Internal tide scattering at seamounts, ridges, and islands. *J. Geophys. Res.*, **108**, 3180, doi:10.1029/2002JC01528.

Klymak, J. M., and S. Legg, 2010: A simple mixing scheme for models that resolve breaking internal waves, doi:10.1016/j.ocemod.2010.02.005, in press for *Ocean Modell.*

Klymak, J. M., S. Legg, and R. Pinkel, 2010: High-mode stationary waves in stratified flow over large obstacles. *J. Fluid Mech.*, **644**, 312–336.

Klymak, J. M., J. N. Moum, J. D. Nash, E. Kunze, J. B. Girton, G. S. Carter, C. M. Lee, T. B. Sanford, and M. C. Gregg, 2006: An estimate of tidal energy lost to turbulence at the Hawaiian Ridge. *J. Phys. Oceanogr.*, **36**, 1148–1164.

Klymak, J. M., R. Pinkel, and L. Rainville, 2008: Direct breaking of the internal tide near topography: Kaena Ridge, Hawaii. *J. Phys. Oceanogr.*, **38**, 380–399.

Lee, C. M., E. Kunze, T. B. Sanford, J. D. Nash, M. A. Merrifield, and P. E. Holloway, 2006: Internal tides and turbulence along the 3000-m isobath of the Hawaiian Ridge with model comparisons. *J. Phys. Oceanogr.*, **36**, 1165–1183.

Legg, S., and A. Adcroft, 2003: Internal wave breaking at concave and convex continental slopes. *J. Phys. Oceanogr.*, **33**, 2224–2246.

Legg, S., and K. M. Huijts, 2006: Preliminary simulations of internal waves and mixing generated by finite amplitude tidal flow over isolated topography. *Deep Sea Research Part II: Topical Studies in Oceanography*, **53**, doi:DOI: 10.1016/j.dsr2.2005.09.014, 140 – 156.

Legg, S., and J. M. Klymak, 2008: Internal hydrualic jumps and overturning generated by tidal flow over a steep ridge. *J. Phys. Oceanogr.*, 1949–1964.

Levine, M. D., and T. J. Boyd, 2006: Tidally-forced internal waves and overturns observed on a slope: results from the HOME survey component. *J. Phys. Oceanogr.*, **36**, 1184–1201.

Llewellyn Smith, S. G., and W. R. Young, 2003: Tidal conversion at a very steep ridge. *J. Fluid Mech.*, **495**, 175–191.

MacKinnon, J. A., and K. B. Winters, 2005: Reconsidering a disqualified candidate for the energy balance of oceanic internal waves, submitted *J. Phys. Oceanog.*

Marshall, J., A. Adcroft, C. Hill, L. Perelman, and C. Heisey, 1997: A finite-volume, incompressible Navier-Stokes model for studies of the ocean on parallel computers. *J. Geophys. Res.*, **102**, 5753–5766.

McComas, C. H., and P. Müller, 1981: Time scales of resonant interaction among oceanic internal waves. *J. Phys. Oceanogr.*, **11**, 139–147.

McPhee, E. E., and E. Kunze, 2002: Boundary layer intrusions from a sloping bottom: A mechanism for generating intermediate nepheloid layers. *J. Geophys. Res.*, **107**, doi:doi:2001JC000801.

Mellor, G. L., and T. Yamada, 1982: Development of a turbulence closure model for geophysical fluid problems. *Rev. Geophys. Space Phys.*, **20**, 851–875.

Merrifield, M. A., and P. E. Holloway, 2002: Model estimate of m_2 internal tide energetics at the Hawaiian Ridge. *J. Geophys. Res.*, **107**, 10.1029/2001JC000996.

Nash, J., M. Alford, E. Kunze, K. Martini, and S. Kelley, 2007: Hotspots of deep ocean mixing on the Oregon continental slope. *Geophys. Res. Lett.*, **34**, L01605, doi:10.1029/2006GL028170.

Nash, J. D., E. Kunze, J. M. Toole, and R. W. Schmitt, 2004: Internal tide reflection and turbulent mixing on the Continental Slope. *J. Phys. Oceanogr.*, 1117–1134.

Naveira Garabato, A. C., K. L. Polzin, B. A. King, K. J. Heywood, and M. Visbeck, 2004: Widespread intense turbulent mixing in the southern ocean. *Science*, **303**, doi:doi:10.1126/science.1090929, 210–213.

Polzin, K., 2004: Idealized solutions for the energy balance of the finescale internal wave field. *J. Phys. Oceanogr.*, **34**, 231–246.

Polzin, K., J. Toole, J. Ledwell, and R. Schmitt, 1997: Spatial variability of turbulent mixing in the abyssal ocean. *Science*, **276**, 93–96.

Polzin, K. L., 2009: An abyssal recipe. *Ocean Modelling*, doi:doi:10.1016/j.ocemod.2009.07.007.

St. Laurent, L., and C. Garrett, 2002: The role of internal tides in mixing the deep ocean. *J. Phys. Oceanogr.*, **32**, 2882–2899.

St. Laurent, L. C., and J. D. Nash, 2004: On the fraction of internal tide energy dissipated near topography. *Near-Boundary Processes and Their Parameterization Proceedings of the 13th 'Aha Huliko'a Hawaiian Winter Workshop, 2003*, P. K. M uller, ed., 45–58.

St. Laurent, L. C., H. L. Simmons, and S. Jayne, 2002: Estimating tidally driven mixing in the deep ocean. *Geophys. Res. Lett.*, **29**, doi:10.1029/2002GL015633.

St. Laurent, L. C., S. Stringer, C. Garrett, and D. Perrault-Joncas, 2003: The generation of internal tides at abrupt topography. *Deep Sea Res. I*, **50**, 987–1003,10.1016/S0967–0637(03)00096–7.

Generated with ametsocjmk.cls.
Written by J. M. Klymak
mailto:jklymak@ucsd.edu
http://opg1.ucsd.edu/ jklymak/WorkTools.html